JOURNAL OF MATERIALS SCIENCE **36** (2001) 1975–1979

Microstructural study of laser-clad Fe-Al bronze on Al-Si alloy

A. H. WANG, C. S. XIE
State Key Lab of Plastic Forming Simulation and Die & Mould Technology, Faculty of Materials Science & Engineering, Huazhong University of Science & Technology, Wuhan, 430074, People's Republic of China
E-mail: pmahwang@public.wh.hb.cn

Microstructure studies of laser-clad Fe-Al bronze on an Al-Si alloy were carried out by OM(optical microscope), SEM(scanning electron microscope), TEM(transmission electron microscope) and XRD(X ray diffraction) analyses. The cross-section of the laser-cladding was divided into clad region and transitional region. The clad region composes a matrix with a twin structure of needle-like and feathery appearance and a second phase of Cu_9Al_4. The transitional region consists of two layers. The layer close to the clad region shows polygonal crystalline while the layer close to the substrate region displays a needle-like structure. XRD analyses show that the main phases in the polygonal crystalline layer and the needle-like structure layer are $Cu_3Al + Cu_9Al_4$ and $CuAl_2 + \alpha$-Al, respectively. Finally, the formation mechanism of two regions was analysed.

1. Introduction

Copper-base alloys are found to be good candidates for improving the wear resistance of aluminium alloys through laser cladding treatment due to their good thermal conductivity, low friction coefficient and good material compatibility with aluminium alloys [1–3]. Y. Liu [4] has reported that the laser cladding of Ni-Al bronze onto an Al-Si alloy by a 10 kW continuous wave CO_2 laser can significantly improve the wear resistance of the aluminium alloy substrate. The hardening mechanism of the coating was found to be the formation of the Cu-base martensite, the precipitation of a hard (Ni, Fe, Cu)Al phase and the presence of dislocations and stacking faults. K. Mori *et al.* [3, 5] have also investigated laser cladding of a Cu-base alloy (Cu-14.9Ni-2.7Si-1.4B) on an Al alloy. The hardness and wear resistance were enhanced due to the formation of hard (Fe, Ni)B, $(Fe, Ni)_2B$, $(Ni, Fe)_5Si_2$, $(Co, Ni, Fe)_3Mo_2Si$ phases by liquid-phase separation when 10wt%Fe + 2wt%B or 10wt%Co + 5wt%Mo were added into the coating. However, in the above investigations, it was found that an inert gas (He or Ar) must be used as the powder carrying gas to protect the laser-generated pool since Al is a reactive metal. In order to melt the fast flow powder stream added into the laser-generated pool efficiently, high-power level CO_2 lasers (over 5 kW) were needed and the low absorption of the Al substrate to the CO_2 laser beam also required the use of high power lasers during the laser cladding process. Our previous investigation showed that an increase in Ni content in Cu-base alloys tends to form more porosity in laser-claddings when the laser cladding treatment was carried out without using shielding gases [6]. When an inert gas was introduced to protect the laser-irradiated zone, porosity-free coatings were produced, even if Cu-base alloys containing a high percentage of Ni were used as the cladding material.

In order to reduce the laser beam energy required for the laser cladding of Al alloys, our previous investigations centred on two aspects [6]: the first was the improvement of the processing method and the second was the development of new coating materials. In the improved processing that we have developed, the powder was delivered to the laser-generated pool by a home-made powder feeding system, in which the powder flowed into the pool only by its own gravity without assistance from the carrying gas. In the improved method, the flow rate of the powder was so slow that the laser beam could melt the powder into the laser-generated pool efficiently. This made it possible for the laser cladding on Al-Si alloy to be achieved by a 2 kW CO_2 laser. In our previous study, a Fe-Al bronze alloy was used as the coating material, which has different composition compared to the coating material (Ni-Al bronze) used by Liu. Results showed that the utilisation of the Fe-Al bronze could avoid the presence of porosity even if the cladding process was carried out without using an inert carrying gas.

The goal of the present study was to understand the microstructure of laser-clad Fe-Al bronze on an Al-Si alloy produced under the improved laser processing condition.

2. Experimental procedure

Compositions of the substrate and the clad powder are given in Table I. Samples for microstructural analysis were laser-clad using the following optimal parameters: laser power $P = 2$ kW, beam diameter $d = 3$ mm,

TABLE I Chemical compositions of the substrate and the cladding powder

	element (wt%)					
Material	Mg	Al	Si	Fe	Ni	Cu
Substrate	2.10	Bal.	13.2	—	1.30	1.30
Cladding	—	8.49	0.3	4.73	—	bal.

scanning velocity Vs = 6 mm/s, relative powder flow rate $G = 20$ mg/mm ($G = V_p/V_s$, Vp is the powder flow rate, mg/s). Nitrogen gas was blown axially to the laser beam axis to protect the focusing lens.

Five tracks of the overlapping claddings were made for SEM/TEM examination and X-ray diffraction analysis for the convenience of sampling. Laser parameters for each single track are the optimal parameters stated above. To minimize the heat effect of the posterior track on the previous ones, the whole substrate was cooled down to the room temperature before the subsequent cladding was carried out and an overlapping ratio of 1/3 was adopted.

The as-clad samples were sectioned into specimens of 10 mm × 10 mm × 8 mm for OM and SEM analysis, and 0.5-mm thick pieces for TEM examination. An etchant of 50 pct HNO_3 and 50 pct CH_3COOH by volume was used to reveal the microstructure for optical microscopy (OM) and SEM (with EDX analysis). For TEM sample preparation, the clad material was first cut into 3-mm-diameter and 0.2-mm-thick discs, which were thinned in a 10 pct H_2SO_4 methanol solution by the twin-jet polishing technique.

An HZG-PC UNIVERSAL type X-ray diffractometer was used for phase analysis in the transitional region. The coatings of as-clad samples were removed by SiC grinding sand paper in direction parallel to the clad, to retain four different thicknesses of coatings, i.e., 0.2 mm, 0.0 mm, −0.1 mm and −0.2 mm. The coating thickness is defined as the distance from the analysed surface to the original substrate surface. Therefore, the places where the coating thickness changed from 0.2 mm to −0.2 mm actually belonged to the transitional region, which was identified by optical microscopy before the XRD test.

3. Results and discussion

A micrograph of the as-polished cross section of a typical crack-free laser cladding is shown in Fig. 1. Three regions were observed, i.e., the clad region (CR), the transitional region (TR) and the substrate region (SR).

SEM observation showed that the morphology of the matrix of the clad region was needle-like appearance with white particles of about 100 nm diameter uniformly-distributed in the matrix, as shown in Fig. 2. Fig. 3 shows a TEM micrograph of the clad region. Needle-like and feathery morphologies were found, as shown in Fig. 3a and b, respectively. The typical twin morphology in the α-Cu matrix is shown in Fig. 4a and b, using bright- and dark-field techniques. The electron diffraction pattern and its indexed results are shown in Fig. 4c and d, respectively. As shown in Fig. 4d, the twin pattern was obtained by selected-area electron

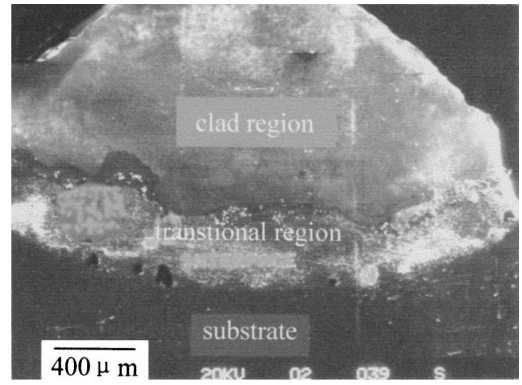

Figure 1 The typical cross section of the laser-cladding showing three regions.

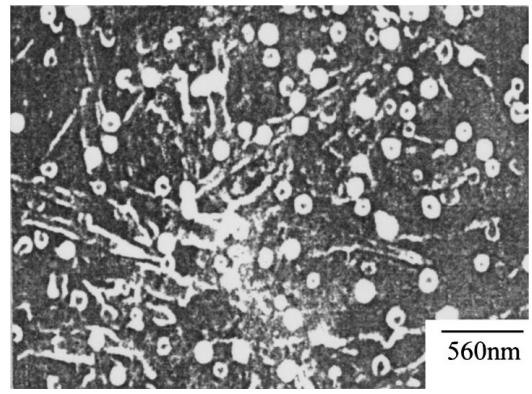

Figure 2 Microstructure of the clad region observed by SEM.

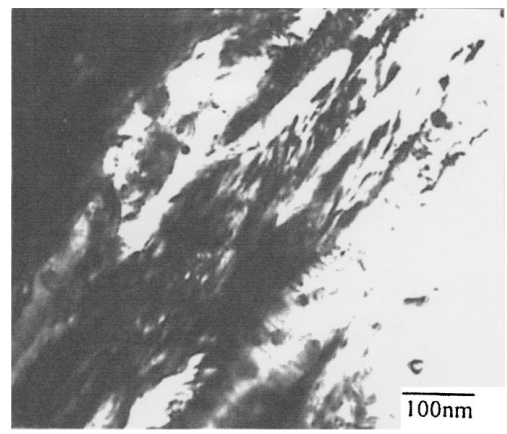

(a)

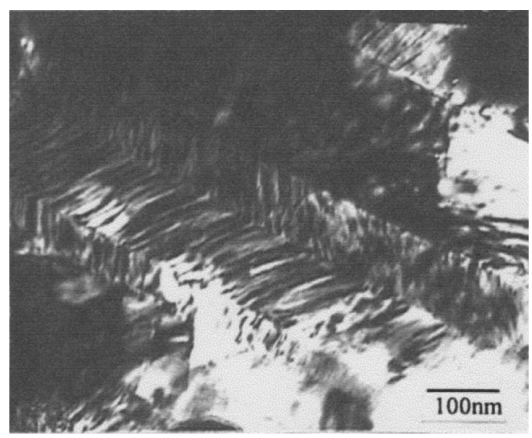

(b)

Figure 3 TEM morphologies of the clad region, (a) α-phase with needle-like appearance, (b) α-phase with feathery appearance.

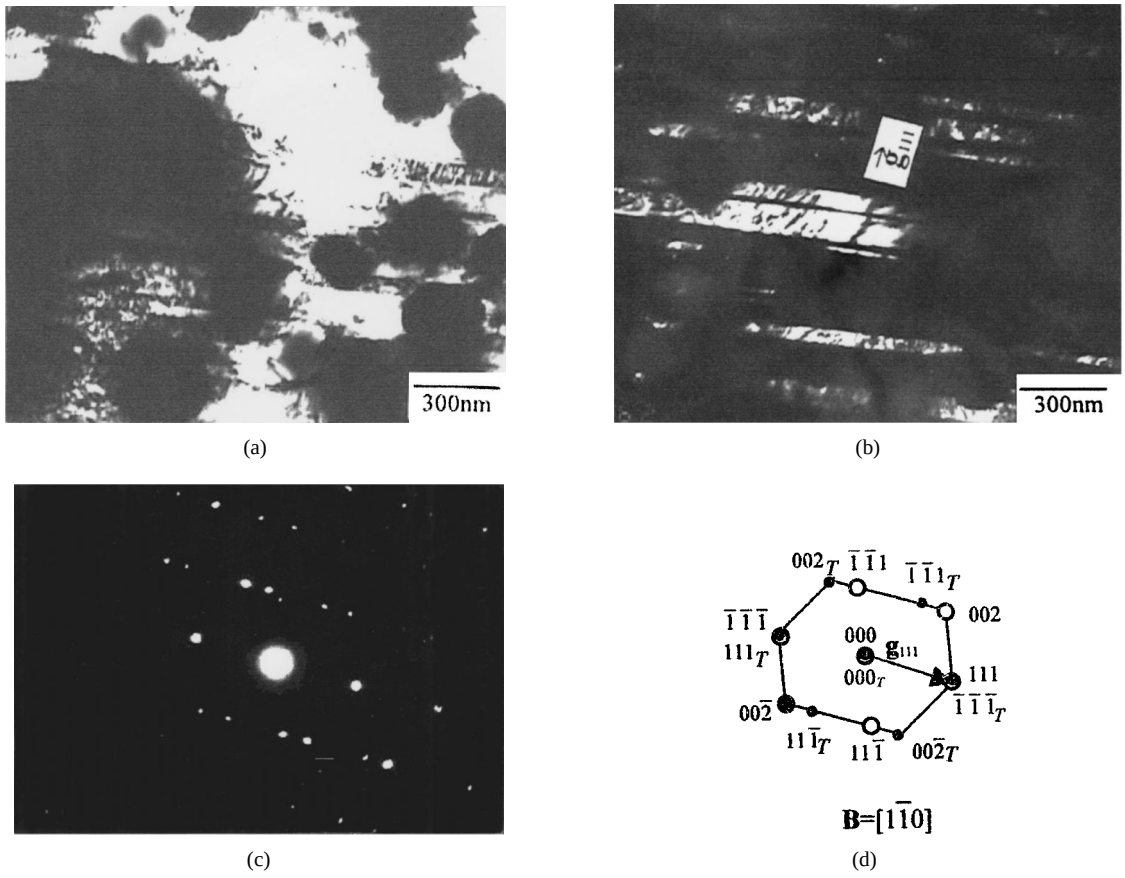

Figure 4 TEM observation of twinning structure: (a) twinning structure shown by bright field, (b) twinning structure by dark field, using the $\mathbf{00\bar{2}_T}$ spot; (c) SAED pattern of twin, and (d) index of (c).

diffraction (SAED) techniques even though there are elongated spots, which was possibly caused by the faulted structure of the α-Cu phase. Both the $\mathbf{111}_T$ and $\mathbf{\bar{1}\bar{1}\bar{1}}_T$ diffraction spots lay at the 1/3 position of the lines between the **002** and **111** or between the **002** and **111** spots, coinciding with the [111] zone axes. $\mathbf{g_{111}}$ was perpendicular to the twin planes shown in Fig. 4b and d. Thus, it is concluded that twinning occurred on the (111) crystal face of the α–Cu. TEM observation of particles in Fig. 2 is shown in Fig. 5a. SAED analysis indicated that the particles were a Cu_9Al_4 type phase with a cubic structure, as shown in Fig. 5b and c. TEM EDX analysis showed that the particle has a composition of 83.82Cu-14.45Al-1.25Fe-0.48Si at wt%. This suggests that a small amount of the Cu in the Cu_9Al_4 type phase was probably substituted by Fe and Si, and to give a particle with the formula $(Cu, Fe, Si)_9Al_4$.

The change in microstructure from the clad region to the substrate region is shown in Fig. 6. Four typical morphologies were found in the transitional region. The microstructure next to the clad region composed a 15 μm-thick fine polygonal crystalline structure while the zone surrounding this exhibited a coarse polygonal crystalline structure (see Fig. 6a). A mixture of needle-like and polygonal crystalline structure was observed (Fig. 6b) near the coarse polygonal crystalline structure, and the zone close to the substrate displayed a needle-like structure (Fig. 6c).

Fig. 7 shows the SEM EDX compositional profile changing from the clad region to the substrate region. The clad region shows a uniform composition distribution while the transitional region shows significant variations in Cu and Al. The zone close to the clad region had a higher copper content (over 50 wt%). This zone is defined as TR I (the first transitional region), in Fig. 7. The reduce in Cu content from the TR I to the substrate region was gradual in the zone named TR II (the second transitional region). OM observation showed that TR I had a polygonal crystalline morphology while that of TR II changed from the mixed polygonal and needle-like crystalline morphology to needle-like crystalline progressively.

Fig. 8 shows the XRD patterns of the samples with different coating thickness. OM observation showed that the coating with a thickness of 0.2 mm was characterised by a polygonal crystalline morphology, and strong peaks of Cu_3Al and Cu_9Al_4 were detected on this surface. This could mean that the main phases in polygonal crystalline structure are probably Cu_3Al and Cu_9Al_4. With decreasing thickness, the relative intensity of Cu_3Al and Cu_9Al_4 becomes smaller while the relative intensity of $CuAl_2$, Al and Si was larger. Thus, it can be deduced that the chief phase of the needle-like crystalline phase was $CuAl_2$. The microhardness of the different microstructures also supports the above, as shown in Table II.

From the equilibrium phase diagram of Cu-Al-Fe ternary alloy system, it is known that the equilibrium phase structures of a Cu-8Al-5Fe bronze alloy are α-Cu and Fe-rich particles[7, 8]. A fast solidification process, such as, laser surface melting treatment, can eliminate

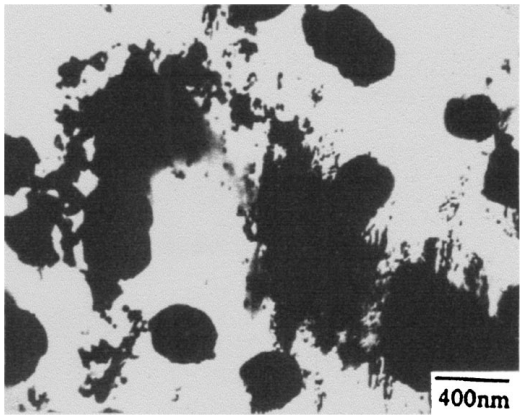

(a)

(b)

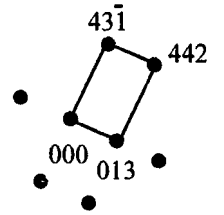

B=[5$\bar{6}$2]
Cu_9Al_4 type phase

(c)

Figure 5 TEM analysis of particles in the clad region (a) typical morphology, (b) SAED pattern of the particle, (c) index of (a).

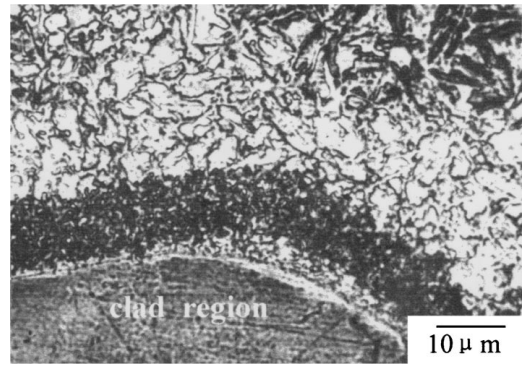

(a)

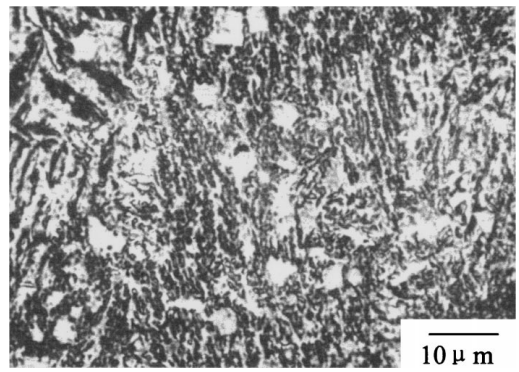

(b)

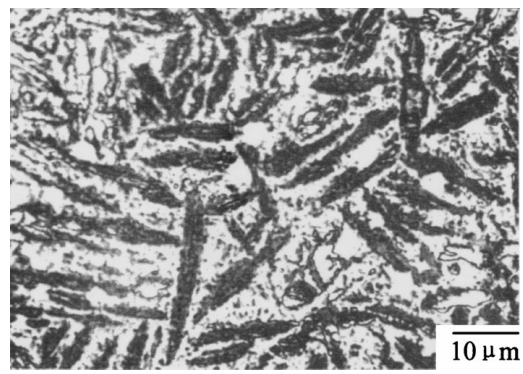

(c)

Figure 6 Microstructure change across the transitional region (a) close to the interface of the clad region and the transitional region (b) intermediate area of the transitional region (c) close to the interface of the transitional region and the substrate region.

Fe-rich precipites [8], and theoretically speaking, the quenching microstructure of a Cu-8Al-5Fe bronze is the martensite with a phase structures of β' and the unvoided phase α [7]. Present result shows that Fe-rich precipitates have also been inhibited owing to the fast solidification of the clad region. However, it is well known that the cooling rate of a laser-irradiated zone

TABLE II Microhardness of the typical microstructures observed in the transitional region and some related aluminides

Microhardness for different microstructures ($HV_{0.1}$)			Microhardness of related aluminides [7]		
Polygonal crystalline	mixed crystalline	needle-like crystalline	Cu_3Al	Cu_9Al_4	$CuAl_2$
687.9, 757.1 619.5, 508.3 657.0, 608.9	426.5, 430, 426, 229.9, 279.6, 295.5	244.3, 273.2, 244.5, 235.6, 305.1, 308.9	∼600	∼1200	∼700

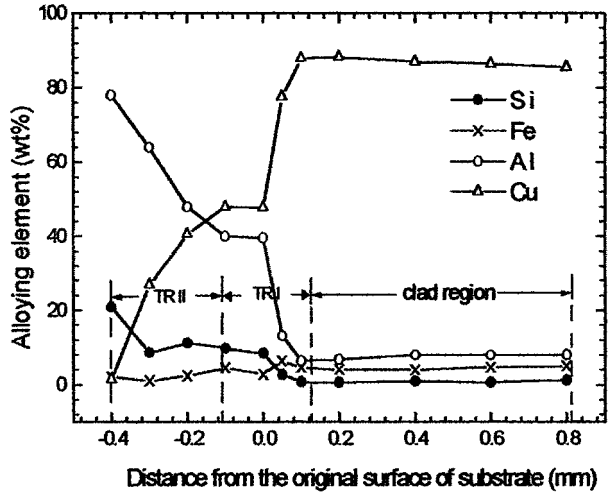

Figure 7 The element distribution along the deep direction of the coaitng.

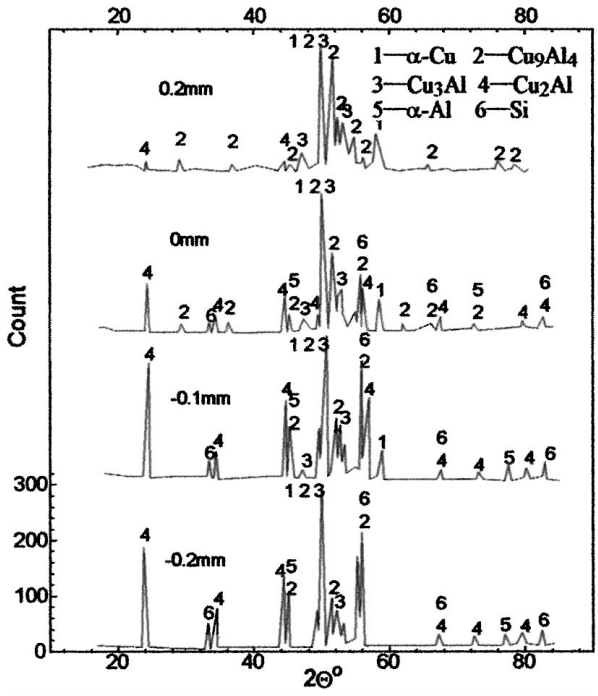

Figure 8 XRD patterns of the transitional region.

is proportional to the scanning velocity. In this study, the scanning velocity is only 6 mm/s due to the usage of lower laser power, which is much lower that that of Liu's and Draper's investigations. As a result, an eutectic reaction from β to $\alpha + Cu_4Al_9$ can not be avoided. Consequently, the phase structures of $\alpha + Cu_4Al_9$ in the laser-clad region have been found.

It is worth to noting that the formation of the transitional region was different from that seen when laser cladding an iron-base alloy onto an aluminium alloy substrate [9]. This phenomenon can be explained from the viewpoint of the property of materials and the thermal history of the solidification process. It is known that the almost full melting of the cladding powder fed into the laser-irradiated zone and a thin layer melting of the substrate surface should be ensured in order to generate a continuous cladding track. This could induce a liquid state mutual diffusion between the melted substrate and the clad material. The high mutual diffusion coefficient and the good miscibility between Al and Cu ensure that the elemental distribution gradually changes from the clad region to the substrate region. During the rapid solidification process, the transitional region comprising α–Al, Cu_9Al_4, Cu_3Al, $CuAl_2$ was generated. The phases were determined by the composition of the melt, of which the Cu-rich phases (such as Cu_9Al_4, Cu_3Al) were found nearby the clad region while Cu-deficient phases (such as α–Al and $CuAl_2$) were generated adjacent to the substrate region. As the liquid/solid interface propagated forward, the release of the latent heat of solidification and the heat of the exothermic reactions caused the remelting of the substrate as well as the remelting of the low melting point phases in the transitional region (such as α–Al and $CuAl_2$), as shown in Table III. The liquid inter-diffusion between the

TABLE III Melting point of some related aluminides [10]

aluminide	Cu_3Al	Cu_9Al_4	Cu_2Al	CuAl	$CuAl_2$
melting point (°C)	1048	1030	950	591	550

remelted substrate and the remelted transitional region and the corresponding solidification resulted in the formation of new transitional region (named transitional region II). At the same time, the portion of the transitional region close to the clad region was unmelted owing to its high melting point (Cu_9Al_4-1030 °C, Cu_3Al-1048 °C), corresponding to the high Cu content portion (called transitional region I), as shown in Fig. 7.

4. Conclusions

1. Three regions have been found in the cross-sections of laser produced Fe-Al bronze coatings on an Al-Si alloy substrate, there are the clad region, the transitional region, and the substrate region.

2. The clad region displays a matrix of twin structure with needle-like or feathery appearance and a second phase of Cu_9Al_4.

3. Crossing the transitional region from the clad region to the substrate region, the morphology gradually changes from a polygonal structure to a needle-like appearance.

4. XRD analysis shows that the phases of the polygonal structure and the needle-like appearance are $Cu_3Al + Cu_9Al_4$ and $CuAl_2 + \alpha$-Al + Si respectively.

Acknowledgement

The authors wish to acknowledge the financial support provided by the Special Foundation for Doctors Research established by the State Education Committee of China.

References

1. Y. LIU, J. MAZUMDER and K. SHIBATA, *Metall. Mater. Trans. B* **25B** (1994) 749.
2. L. POIRE and E. BLANK, *Journal de Physique IV* **4** (1994) C4.
3. K. TANAKA, T. SAITO, Y. SHIMURA, K. MORI, M. KAWASAKI, M. KOYAMA and H. MURASE, *J. Japan Inst. Metals* **57**(10) (1993) 1114.
4. Y. LIU, J. KOCH and J. MAZUMDER, *Metall. Mater. Trans. B* **25B** (1994) 425.
5. M. KAWASAKI, K. TAKASE, S. KATO, M. NAKAGAWA, K. MORI, M. NEMOTO, S. TAKAGI and H. SUGIMOTO, in Proc. Conf. "International Congress & Exposition," Detroit, Michigan, February 1992, SAE Technical Paper Series 920571.
6. A. H. WANG, C. S. XIE, W. HUANG and C. Y. XU, *Rare Metal Materials and Engineering* **26**(6) (1997) 41.
7. P. BREZINA, *International Metals Reviews* **27**(2) (1982) 77.
8. C. W. DRAPER, *J. Mater. Sci.* **16** (1981) 17774.
9. A. H. WANG, C. S. XIE and J. H. NIE, *Materials Science & Technology* **15**(8) (1999) 957.
10. B. P. BABOB, "Welding of Aluminium and Its Alloys with Other Metals" (Yuhang Press, Beijing, 1990) p. 20.

Received 23 February
and accepted 14 August 2000